Anti-fouling piezoelectric PVDF membrane: Effect of morphology on dielectric and piezoelectric properties

Yu Ping Su[a,b], Lee Nuang Sim[a], Xin Li[a], Hans G.L. Coster[c], Tzyy Haur Chong[a,d,*]

[a] Singapore Membrane Technology Centre, Nanyang Environment and Water Research Institute, Nanyang Technological University, 1 Cleantech Loop, CleanTech One #06-08, Singapore 637141, Singapore

[b] Interdisciplinary Graduate School, Nanyang Technological University, 50 Nanyang Avenue, Singapore 639798, Singapore

[c] School of Chemical and Biomolecular Engineering, University of Sydney, Sydney, NSW 2006, Australia

[d] School of Civil and Environmental Engineering, Nanyang Technological University, 50 Nanyang Avenue, Singapore 639798, Singapore

*Corresponding author: E-mail: thchong@ntu.edu.sg (T.H. Chong)

ABSTRACT

Piezoelectric membrane serves as an alternative to vibratory shear-enhanced process, which potentially offers lower cost of operation as the source of agitation is the membrane itself. The effect of morphology on dielectric and piezoelectric properties of polyvinylidene fluoride (PVDF) membranes prepared via non-solvent induced phase separation method was investigated. The membranes were fabricated using different solvents: N,N-dimethylformamide (PVDF-DMF), 1-methyl-2-pyrrolidinone (PVDF-NMP) and triethyl phosphate (PVDF-TEP). Dielectric strength analysis and piezo-response force microscopy (PFM) revealed that PVDF-DMF, displaying finger-like morphology, presented highest dielectric strength and desired piezoelectric properties. The presence of macrovoids in PVDF-NMP resulted in weak dielectric strength. Electrical poling was performed, enhancing the piezoelectric properties of membranes. No noticeable change in microstructure was observed for PVDF-NMP after poling. However, cross-section morphology of PVDF-DMF visibly changed from finger-like to drop-like cavities. Infrared (IR) spectroscopy and PFM showed improvements in fraction of β phase and piezoelectric coefficient d_{33} after poling. Cross-flow filtration experiments using colloidal silica were performed to investigate effect of electrical signal (10 Vpp, 500 Hz) on the membranes. It showed negligible effect on performance of unpoled PVDF-DMF, while 46% increase in critical flux and 66% reduction in transmembrane pressure increase (dTMP/dt) was observed for poled PVDF-DMF under electrical signal.

Keywords: Piezoelectric membrane, Piezo-response force microscopy, Polyvinylidene fluoride, Non-solvent induced phase separation, Fouling

1. Introduction

Membrane fouling is the major challenge of membrane technology and is inevitable during long term operation. Common approaches applied to prevent or to mitigate membrane fouling include pre-treatment to reduce the foulant load entering the membrane system, addition of anti-fouling chemicals, and employment of unsteady-shear. The unsteady-shear methods include gas sparging, vibrating membranes, particle fluidizing and flow pulsations [1]. Vibratory shear-enhanced process (VSEP), an example of unsteady-shear methods, has been commercialized for industrial applications by New Logic Research and has been used in different types of membrane modules spanning from microfiltration to reverse osmosis [2, 3, 4]. In VSEP, the maximum achievable shear rate is approximately 10^5 s^{-1} which is significantly higher than gas sparging. However, one of the limitations of VSEP is its unattractive energy consumption, where specific power of 500 W/m^2 has been reported [1]. Recently, the construction of a novel membrane that possessed piezoelectric properties has been proposed [5, 6, 7, 8]. Instead of tangential shear due to mechanical vibration, piezoelectric membrane itself serves as the source of agitation when it undergoes internal vibrational deformations normal to the plane [9].

Polyvinylidene fluoride (PVDF) is a semi-crystalline polymer, which is an ideal material for fabricating piezoelectric membrane due to its piezoelectric properties [10]. Moreover, owing to its superior chemical and mechanical resistance, PVDF is an attractive polymer for membrane fabrication via phase inversion techniques [11]. Among the four known crystalline structures (α, β, γ, δ) of PVDF polymer, all-trans (β) phase is the primary contributor for piezoelectric properties of PVDF [12]. Zhang et al. [13] reported that PVDF membranes with mainly β phase demonstrated superior fouling resistance as compared to PVDF membranes with mainly α phase. However, the commonly used fabrication methods (e.g. melt or solution techniques) induce the dominant non-piezoelectric α phase in PVDF structure [14], which significantly compromised its piezoelectric property. Therefore, many research works have devoted to study the formation of β phase of PVDF by different approaches, such as addition of additives [15], annealing [16, 17], crystallization under high pressure [18], electrical poling [19], mechanical stretching [14], and polymer blending [20, 21]. Among them, electrical poling is a common strategy to convert crystalline structure of PVDF from α phase into β phase where the PVDF dipoles orientate themselves in the direction of the electric field. With this strategy, previous studies on piezoelectric membranes were based on commercial flat sheet PVDF membranes proposed [5, 6, 7, 8, 22], electrospun PVDF nanofiber membranes [23, 24] and piezoceramic membranes [25, 26, 27]. These piezoelectric membranes showed improved filtration performance under the application of AC signal or ultrasound. For example, Coster et al. [5] using poled commercial flat sheet PVDF membrane, reported an average flux improvement of 136 % for filtration of 1 % polyethylene glycol. They found that the energy requirement for operating piezoelectric flat sheet PVDF membrane was 110 W/m^2, which was only 20 % of that of VSEP [7]. Bae et al. [23] prepared piezoelectric electrospun PVDF nanofiber membranes and found that for membranes under AC signal, the flux decline was reduced by 15 % for filtration of 10 ppm alginate solution. Mao et al. [26] synthesized lead zirconate titanate (PZT) membranes and poled the membranes in mineral oil. Normalized membrane permeance of poled PZT membranes was raised by 15 to 20 % for filtration of 500 ppm oil-in-water emulsion. Cao et al. [28] fabricated flat sheet PVDF membranes via thermally induced phase separation (TIPS) and the membranes were electrically poled for application in anaerobic membrane bioreactor. It was shown that steady-state water flux of piezoelectric PVDF membrane under electrical signal was enhanced by 72.6 % as compared to non-piezoelectric membranes.

Even though the improved filtration performance has been confirmed with poled PVDF membrane, membrane properties such as morphology and polymorphism that affect the piezoelectric properties of the membrane have yet to be explored. Different membrane morphologies could be obtained by adjusting the solvent types for phase inversion of polymer solution [29]. The degree of miscibility between solvent and nonsolvent during phase inversion affected the solvent-nonsolvent exchange rate which in turn resulted in different morphologies [30]. A poor miscibility of solvent and nonsolvent led to slow solvent-nonsolvent exchange which resulted in sponge-like morphology whilst a good miscibility of solvent and nonsolvent lead to fast solvent-nonsolvent exchange which resulted in finger-like structure. Tao et al. [31] investigated on the effect of different solvents on membrane polymorphism and found that the polymorphism of PVDF membranes was primarily determined by the extent of dissolution of PVDF in each solvent. Phase inversion of polymer solution in which the PVDF was well dissolved, formed membranes with α phase, while poorly dissolved PVDF solutions formed membranes with β phase. Darestani et al. [32] studied the electric breakdown behaviour of a wide range of commercial membranes and concluded that membrane morphology was a key factor that determined the dielectric strength or electric breakdown behaviour of the membranes. Furthermore, the presence of pores and defects in PVDF membranes may cause electrical breakdown during poling.

In this study, flat sheet PVDF membranes with different morphologies were fabricated by using different solvents via non-solvent induced phase separation (NIPS). The effects of these morphologies on the dielectric and piezoelectric behaviour of the membranes were explored. Electrical poling was then performed on the PVDF membranes to further improve its piezoelectric properties. Filtration performances of the unpoled and poled membranes were investigated.

2. Experimental

2.1. Materials

PVDF (Solef® 6020) was supplied by Solvay Specialty Polymers and it was dried in a vacuum oven at 60 ^{o}C prior to use. N,N-dimethylformamide (DMF, anhydrous, 99.8 %, Sigma-Aldrich), 1-methyl-2-pyrrolidinone (NMP, anhydrous, 99.5 %, Sigma-Aldrich) and triethyl phosphate (TEP, ReagentPlus®, ≥ 99.8 %, Sigma-Aldrich) were used as solvents to fabricate the PVDF membranes. All the chemical reagents were utilized without further purification. Commercial PVDF membranes, that were used for comparison, were supplied by Synder Filtration (250 kDa UF BX PVDF). These membranes are referred to as UF-Synder in the subsequent sections.

For membrane fouling tests, colloidal silica was selected as model foulant. Test solution contains 200 mg/L of silica was prepared from LUDOX® TMA colloidal silica (Sigma-Aldrich). The colloidal silica was supplied in the form of 34 wt% in deionised water at pH 7.0. No significant change in the pH was detected upon the addition of silica to the test solution, which remained at pH 6.5 ± 0.5 throughout the experiment. The nominal size of silica particles was 22 nm based on the datasheet provided by the manufacturer.

2.2. Preparation of PVDF membranes

PVDF membranes were prepared via NIPS process. The solvents used to separately prepare the polymer solutions were DMF, NMP and TEP. 15 wt.% PVDF powder was dissolved in each solvent at 80 ^{o}C under constant rate of stirring to form a homogeneous dope solution. The dope solution was then left still at 25 ^{o}C for 12 h for degassing. The degassed solution was uniformly spread onto a glass plate by a casting knife (Elcometer) set with gap thickness of 250 µm to form an incipient membrane. Subsequently, the glass plate was immersed into a coagulation bath of deionized (DI) water (nonsolvent) at 25 ^{o}C. Once peeled off from the glass plate, the solidified membranes were transferred into a fresh DI water bath and stored for 24 h to remove residual solvent. The membranes were then freeze-dried. The three types of fabricated membranes were termed as PVDF-DMF, PVDF-NMP and PVDF-TEP, i.e. PVDF-DMF refers to PVDF membrane fabricated using DMF as the solvent.

2.3. Membrane characterization

2.3.1. Scanning electron microscopy

The morphology and thickness of the membrane samples were examined using a field emission scanning electron microscope (FESEM, JOEL JSM-7200F Schottky). Prior to FESEM analysis, the samples were coated with 2-nm of platinum layer via the sputtering technique. The average thickness of the membranes was reported based on five separate measurements.

2.3.2. Dielectric strength analysis

The dielectric strength of a sample is defined as the electrical breakdown voltage divided by its thickness. To determine the electrical breakdown voltage, a 30 mm × 30 mm rectangular membrane sample was sandwiched between two stainless steel electrodes at room temperature. The potential difference across the membrane was then slowly raised at a rate of 50 V/min until the membrane was charred at a particular spot which caused the overload in the high voltage power supply to trip. Electrical arcing around the edge of the membrane was prevented by using a smaller top electrode (20 mm × 20 mm) as compared to bottom electrode (200 mm × 200 mm). An average dielectric strength was calculated for each sample based on five different measurements.

2.3.3. Piezo-response force microscopy

Piezo-response force microscopy (PFM) was performed using the PFM scanning mode on an atomic force microscope (Park Systems, Park NX 10). PFM was operated in contact mode.

Beside PFM amplitude and PFM phase images, topography images were also produced to characterize the average surface roughness of the membranes. In PFM imaging, an electrically conductive cantilever with tip coated with Chromium/Platinum (force constant of 3 N/m, resonance frequency of 75 kHz) was brought into contact with the surface of the sample. An alternating current (AC) bias of 8 V riding on a direct current (DC) bias of −8 V was applied between the cantilever tip and the bottom electrode. A total of 256 × 256 pixels was measured for a scan area of 2 μm × 2 μm. The piezoelectric coefficient d_{33}, was determined by performing piezoelectric response spectroscopy and applying Eq. (1):

$$d_{33} = \frac{3 \times \text{PFM Amplitude}}{(A - B)\text{Sensitivity} \times (A + B)\text{DC} \times \text{Tip Bias}} \tag{1}$$

where PFM Amplitude (mV) is the maximum amplitude obtained on the amplitude-voltage hysteresis loop as shown on Fig. 1, $(A - B)$Sensitivity is the sensitivity of the cantilever with value of 33.333 V/μm, $(A + B)$DC is the intensity of the laser beam which was aligned prior to scanning with values that ranged between 3 and 4, and Tip Bias is the applied AC tip bias which was set at 10 V. It should be pointed out that PFM imaging and piezoelectric response spectroscopy are two different techniques and their settings were different as mentioned above.

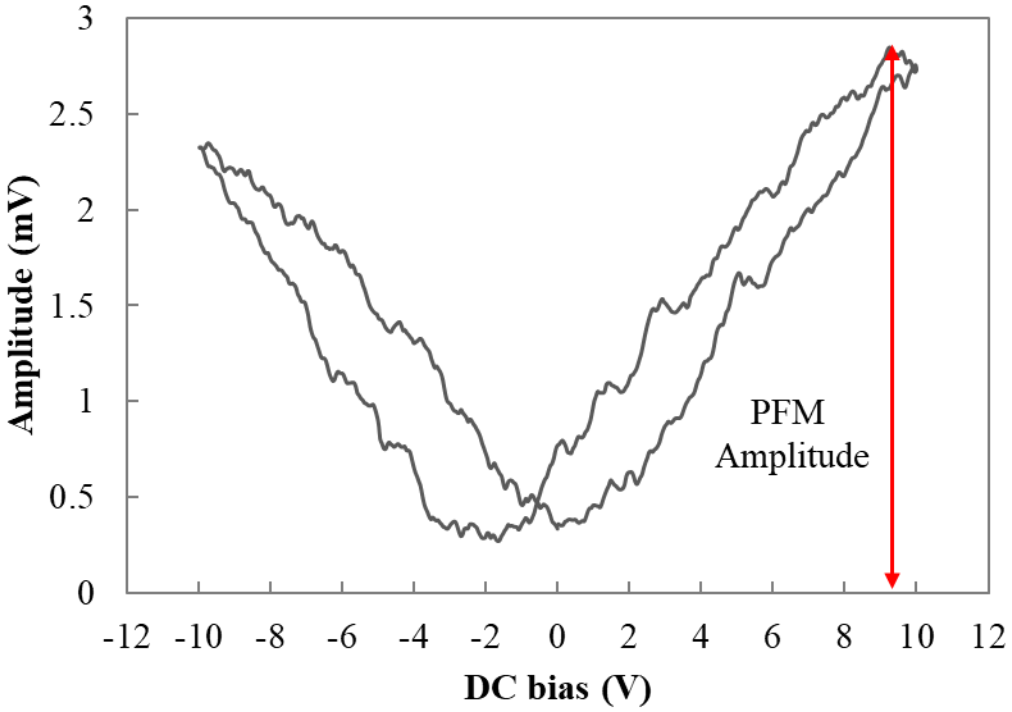

Fig. 1: An example of the amplitude-voltage hysteresis loop of a PVDF membrane. PFM (Piezo-response force microscopy) amplitude in Eq. (1) refers to the maximum amplitude of the amplitude-voltage hysteresis loop as depicted by the arrow.

During piezoelectric response spectroscopy, tip deflection was detected while applying a DC bias sweep (−10 V to +10 V) and fixed AC bias on the sample and tip respectively. Tip deflection was expressed in terms of PFM amplitude as shown in Fig. 1. Note that Eq. (1) was given by Park Systems and it is only applicable to NX systems provided by Park Systems.

2.3.4. Infrared spectroscopy

The crystalline phase in the membrane sample was investigated by infrared (IR) spectroscopy. The IR spectrum of a sample was obtained using a Shimadzu IRPrestige-21 fourier-transform infrared spectroscopy (FTIR) spectrometer in an attenuated total reflectance mode. IR spectra were measured in the range of 400 to 1,500 cm^{-1} at room temperature of 25 ^{o}C. The relative fraction of β phase ($F(\beta)$) was calculated using Eq. (2) [33]:

$$F(\beta) = \frac{A_\beta}{\frac{K_\beta}{K_\alpha} A_\alpha + A_\beta} \qquad (2)$$

where A_α and A_β are the absorbance values at 763 cm^{-1} and 840 cm^{-1} respectively while K_α and K_β are absorption coefficients with values of 6.1×10^4 and 7.7×10^4 cm^2.mol^{-1} respectively. IR absorption peaks, at 763 cm^{-1} and 840 cm^{-1}, are characteristic peaks of α and β phases respectively [33]. The average $F(\beta)$ was calculated based on five different measurements for each membrane.

2.3.5. Mechanical strength analysis

The mechanical properties of the membranes were characterized by a universal testing machine (Instron 5567 electromechanical tester). The membrane sample was clamped using the tensile grips and pulled longitudinally at a rate of 20 mm/min at room temperature. The test was repeated three times to get average values for each sample.

2.3.6. Evapo-porometry

Mass-based pore diameter and porosity of a membrane sample were determined using evapo-porometry (EP) [34]. This technique is based on the Kelvin equation that relates the evaporation rate of volatile liquid to the pore diameter. The membrane sample was wetted using ethanol (ethanol absolute EMSURE® ACS, Merck) after placing it into the EP cell. The cell was then stationed in an incubator (LE-150D, Yihder Technology) maintained at 28.0 ± 0.1 ^{o}C. Evaporation of free-standing ethanol layer occurred first, followed by evaporation of ethanol from the membrane pores. The gravimetric data were measured semi-micro balance (ME235S, Sartorius) and logged on a computer. The evaporation rate was then calculated based on the gravimetric data. The onset of pore draining was indicated by deviation of evaporation rate from initial constant evaporation rate. Membrane porosity was determined using Eq. (3) [35]:

$$\text{Porosity}(\%) = \frac{\frac{m_{wet} - m_{dry}}{\rho_w}}{\frac{m_{wet} - m_{dry}}{\rho_w} + \frac{m_{dry}}{\rho_m}} \times 100\ \% \tag{3}$$

where m_{wet} is the mass of the wetted membrane before pore draining, m_{dry} is the mass of the dry membrane, ρ_w is the density of the wetting liquid (0.789 g/cm^3), and ρ_m is the density of the membrane. The average pore diameter and porosity were determined by three separate measurements.

2.4. Electrical poling setup

Piezoelectric properties of PVDF membranes were enhanced by electrical poling. During electrical poling, a 90 mm × 90 mm PVDF membrane was placed between two stainless steel electrodes as illustrated in Fig. 2.

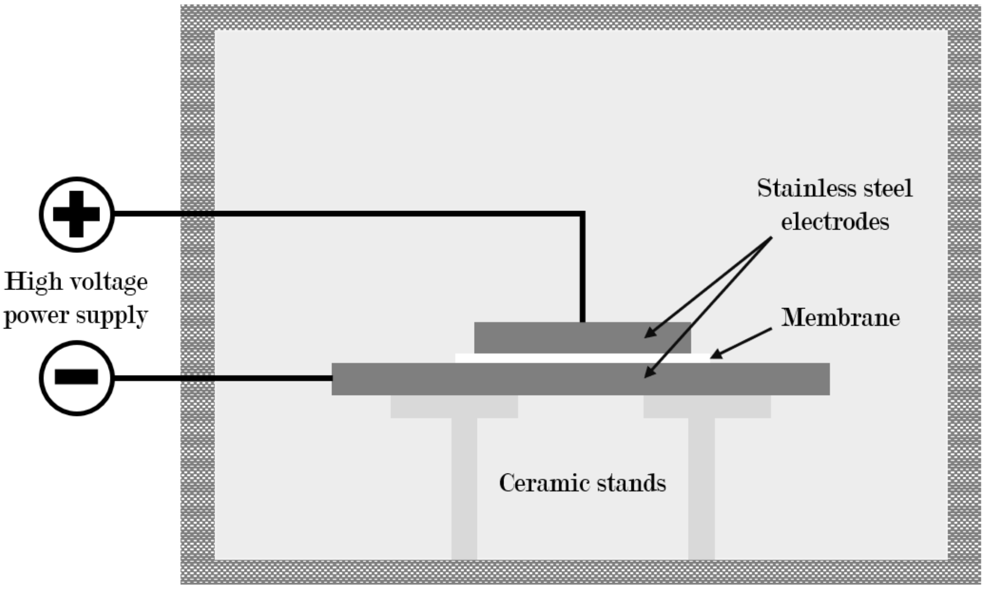

Fig. 2: Electrical poling setup enclosed within the oven.

The membrane sample was heated in the oven from ambient temperature to 50 ± 5 ^{o}C. Membranes were poled in the oven to ensure uniform heating. Once the desired temperature was achieved, the potential difference between the two electrodes was gradually increased from

0 V to the desired value at a rate of 50 V/min. A high voltage DC power supply (Stanford Research Systems, model PS375) was used to achieve the required potential difference across the membrane. Thereafter, the membrane sample was held at these conditions for a duration of 2 h. The oven was then switched off to allow the membrane sample to cool till ambient temperature while the voltage was still applied. Once it was cooled, the voltage was steadily decreased to 0 V at a rate of 50 V/min. Since the top electrode (80 mm × 80 mm) was smaller than the bottom electrode (200 mm × 200 mm), only the portion of the membrane exposed to the intense electric field between the two electrodes was used for membrane characterization and filtration experiments.

The poling temperature was set at 50 ^{o}C while the poling voltage varied among different types of membranes because of the differences in membrane thickness. The desired electric field strength to be applied across the membrane was 10 MV/m (megavolts per meter). Darestani et al. [32] reported that an electric field of approximately 10 MV/m was required to change the microstructure of membranes. However, some of the membranes, such as UF-Synder and PVDF-NMP, could not withstand such high electric field strength. In these cases, the electric field strength was lowered such that electrical breakdown does not occur as shown in Table 1. If electrical breakdown occurred, poling would be terminated as the high voltage power supply was tripped. The occurrence of electrical breakdown could be due to voids and possible defects that exist in the membrane [5].

Table 1: Poling conditions of different types of membranes.

	Temperature (^{o}C)	Potential difference (V)	Electric field strength (MV/m)
UF-Synder	50	500	2
PVDF-DMF	50	500	10
PVDF-NMP	50	650	7
PVDF-TEP	50	800	10

2.5. Filtration performance analysis

The filtration performance of the membranes was tested using a stainless steel cross-flow cell with an effective membrane area of 16.25×10^{-4} m^2. As shown in Fig. 3a, the filtration system comprised of a feed tank (5 L), a temperature control system (9106AA2P, PolyScience), a gear pump (Masterflex® L/S® Standard Digital Drives, Cole-Parmer), three pressure gauges (302174SD02L100, Ashcroft), a signal generator (AFG1022, Tektronix) connected to the cross-flow filtration cell, a mass flow controller (L30C5I, Bronkhorst) located on the permeate stream and a data acquisition system (LabVIEW, National Instruments).

To determine the pure water permeability (PWP) of each sample, the feed pressure was set at approximately 300 kPa and the permeate flux was varied to obtain five different transmembrane pressure (TMP) data. The PWP was calculated as the gradient of the plot of permeate flux against TMP. For each membrane, the test was repeated three times to obtain an average PWP.

During fouling tests, the filtration setup was operated as a closed system in which both permeate and retentate were recycled back into the feed tank. The temperature of the feed (200 mg/L silica solution) was kept constant at 25 ± 1 °C via chiller and the cross-flow velocity was fixed at 0.1 m/s. To investigate the effect of electrical signal on the filtration performance of the unpoled and poled membranes, AC signals of 10 V peak-to-peak (Vpp) and 500 Hz were applied to the filtration cell via the signal injecting points as shown in Fig. 3b [7].

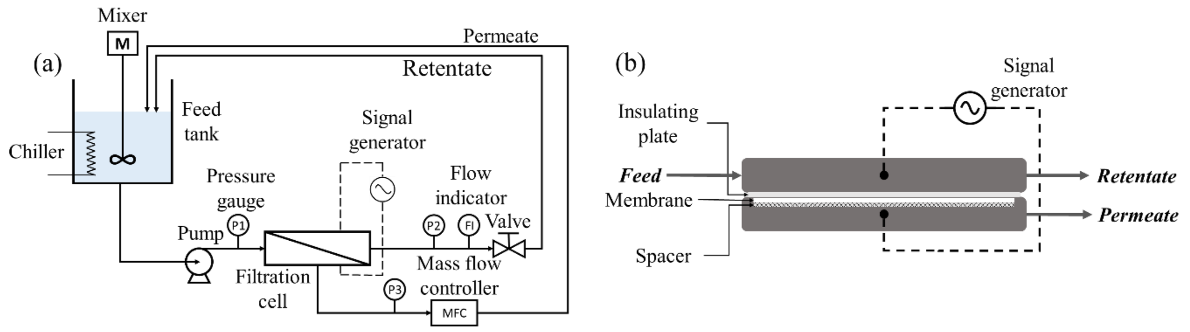

Fig. 3: (a) Process flow diagram of the filtration system and (b) schematic diagram of the cross-flow filtration cell used for filtration tests.

3. Results and discussion

3.1. Effect of morphology on dielectric strength

PVDF membranes with different morphologies were fabricated by using three solvents: DMF, NMP and TEP. These solvents have different solubility for PVDF which led to membranes with different morphology and polymorphism [29, 31, 36, 37]. During fabrication, the gap between the casting knife and the glass plate, and the speed of the casting knife were consistent for all the membranes. The resulting film thickness depends on the viscosity of the polymer solution as shown in elastohydrodynamic film thickness regression equation, Eq. (4) [38]:

$$h = kU^{0,67}\eta^{0.67} \tag{4}$$

where h is the film thickness, U is the rolling speed and η is the dynamic viscosity of the solution at atmospheric pressure. Hence, the varied thicknesses of the resulting membranes were due to the viscosity of the polymer solution. Fig. 4 compares the FESEM images of the top surface and entire cross-section of commercial and fabricated PVDF membranes before and after poling. The explanation of the morphology change after poling could be found in section 3.3.

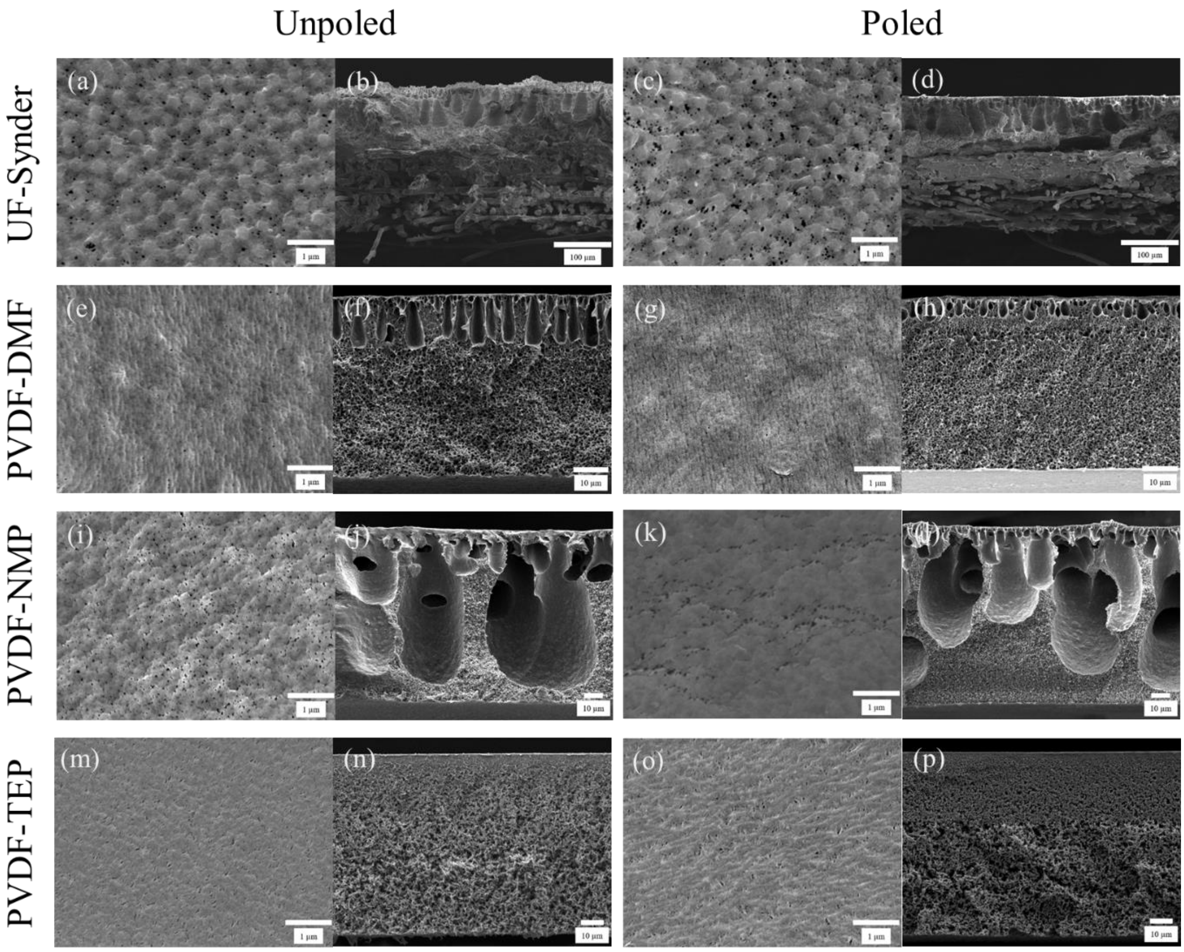

Fig. 4: FESEM images of the top surface and cross-section of unpoled and poled UF-Synder (a, b, c and d), PVDF-DMF (e, f, g and h), PVDF-NMP (i, j, k and l) and PVDF-TEP (m, n, o and p). FESEM images of the top surface are at 20 000 times magnification. FESEM images of the cross-section are at 250, 1 500, 800 and 1 000 times magnification respectively for UF-Synder, PVDF-DMF, PVDF-NMP and PVDF-TEP.

For commercial UF-Synder membranes, Fig. 4a and Fig. 4b reveal that it consisted of spherulites on its top surface and macrovoids with a support layer in its cross-section. The porous top skin layer of commercial UF-Synder membrane resulted in high permeability of UF-Synder membrane as shown in Table 2. The fabricated PVDF-DMF exhibited a dense skin layer with minimally visible pores on its top surface (Fig. 4e) and short finger-like cavities with sponge-like sublayer in the cross-section structure (Fig. 4f). In the case of fabricated PVDF-NMP, large and irregular voids can be observed in Fig. 4j. Conversely, membranes casted with

TEP solvent exhibited asymmetrical sponge-like structures that was denser nearer to the top surface as depicted in Fig. 4n.

The results of the dielectric strength analysis are listed in Fig. 5. The influence of membrane morphology on dielectric strength can be deduced by comparing different morphologies with their respective dielectric strengths.

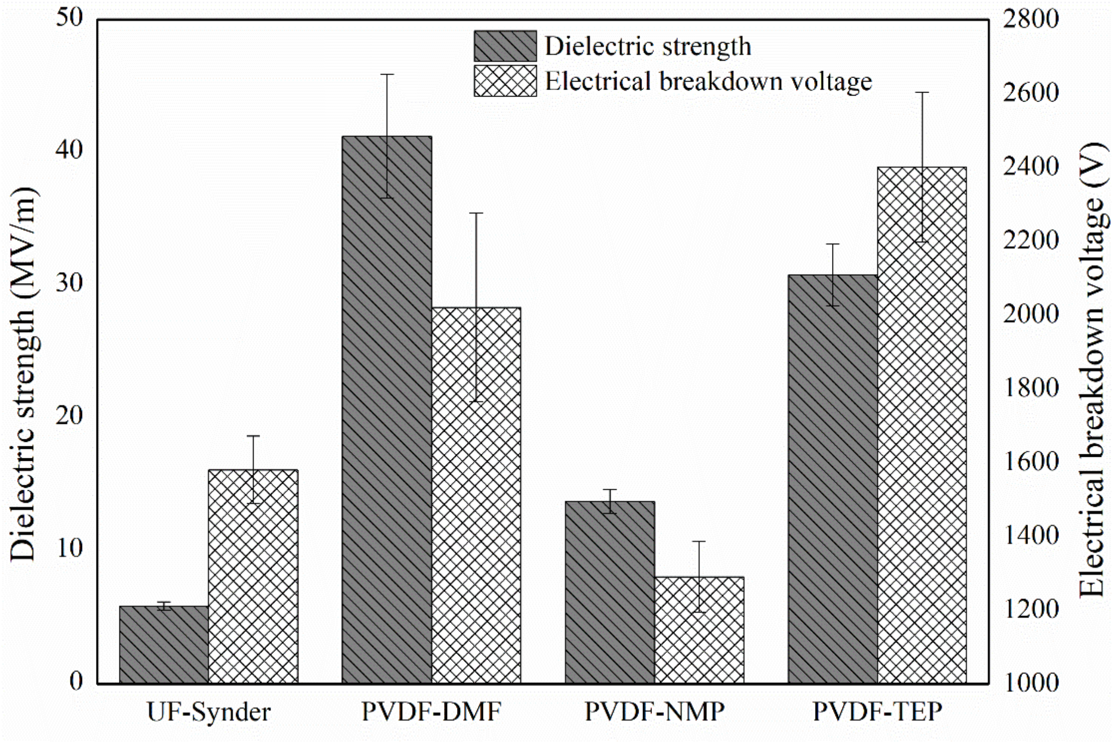

Fig. 5: Dielectric strength (MV/m) of the commercial and fabricated PVDF membranes.

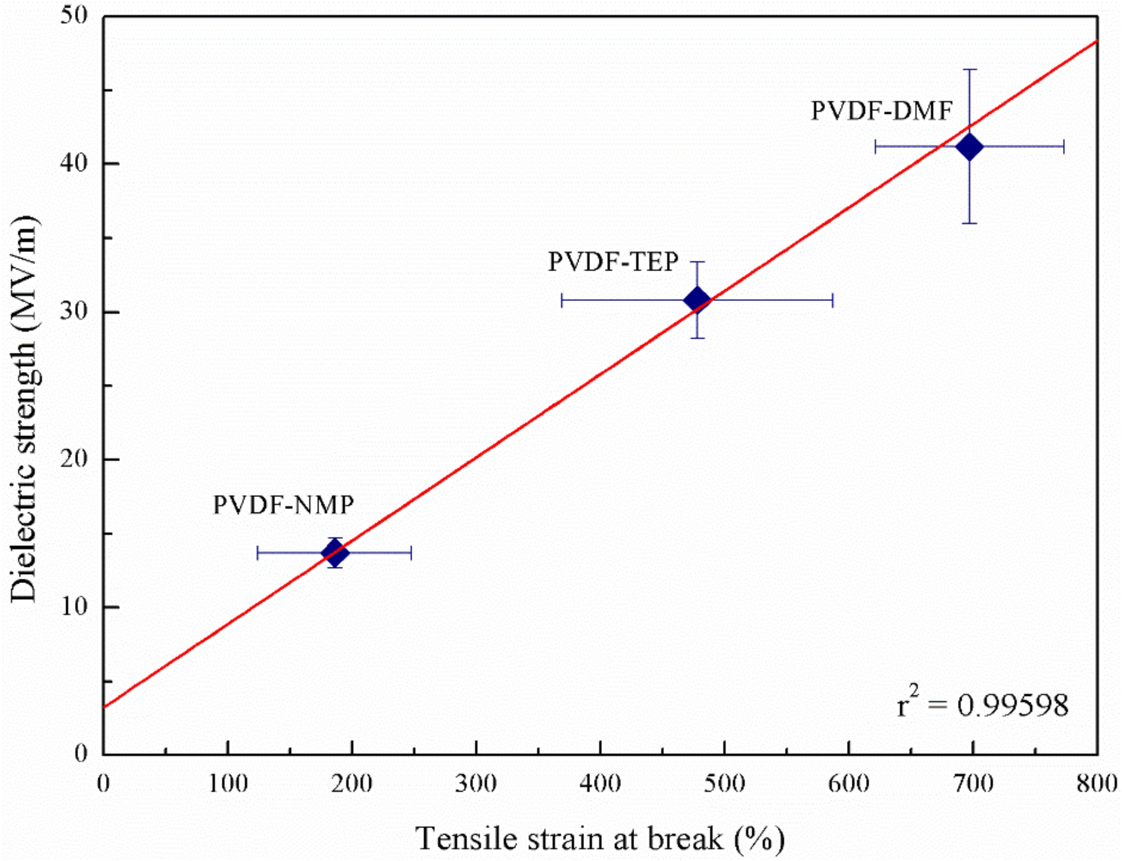

Fig. 6: Plot of dielectric strength (MV/m) against tensile strain at break (%) for unpoled fabricated PVDF membranes.

Table 2: The properties of unpoled and poled UF-Synder, PVDF-DMF, PVDF-NMP and PVDF-TEP.

	Unpoled				Poled			
	UF-Synder	PVDF-DMF	PVDF-NMP	PVDF-TEP	UF-Synder	PVDF-DMF	PVDF-NMP	PVDF-TEP
Membrane properties								
Pore diameter (nm)	57 ± 1	51 ± 7	72 ± 2	81 ± 14	64 ± 7	49 ± 2	69 ± 10	60 ± 10
Porosity (%)	34.8 ± 0.4	71.8 ± 4.1	75.9 ± 2.8	69.2 ± 0.2	47.8 ± 1.0	68.7 ± 0.7	61.0 ± 3.9	57.4 ± 0.9
Thickness (μm)	278 ± 6 (112 ± 9[a])	49 ± 1	94 ± 4	78 ± 2	234 ± 5 (108 ± 6[a])	48 ± 1	91 ± 2	78 ± 1
Permeability (L/m^2.h.bar)	1287 ± 170	61 ± 6	277 ± 32	362 ± 7	2117 ± 77	60 ± 2	259 ± 43	308 ± 49
Average surface roughness (nm)	32	40	36	66	21	33	21	20
Mechanical properties								
Young’s modulus (MPa)	227.8 ± 12.5	119.1 ± 4.8	41.5 ± 1.8	60.0 ± 10.7	459.5 ± 28.9	136.5 ± 4.8	43.1 ± 1.6	40.1 ± 3.4
Tensile strength at break (MPa)	16.6 ± 0.8	13.0 ± 0.5	3.0 ± 0.4	4.3 ± 0.3	32.1 ± 1.4	13.0 ± 2.0	3.2 ± 0.1	2.9 ± 0.1
Tensile strain at break (%)	32 ± 2	697 ± 76	186 ± 62	478 ± 109	29 ± 2	677 ± 111	182 ± 20	273 ± 97
Piezoelectric properties								
Number of points where hysteresis loops were observed	94	87	53	47	62	93	76	62
Average d33 (pm/V)	5.15 ± 3.36	3.25 ± 0.41	3.29 ± 0.70	2.18 ± 0.58	5.13 ± 2.35	3.38 ± 0.45	3.71 ± 1.35	2.73 ± 0.20
$F(\beta)$	0.884 ± 0.005	0.493 ± 0.020	0.509 ± 0.007	0.259 ± 0.019	0.886 ± 0.004	0.504 ± 0.004	0.549 ± 0.012	0.266 ± 0.009

[a] This refer to the thickness of PVDF layer in UF-Synder.

Among the four different membranes referred to in Fig. 5, commercial UF-Synder showed the lowest dielectric strength. This is likely due to the presence of two layers of PVDF and a non-woven support which coincides with findings from another study where they reported discontinuities within membranes led to early electrical breakdown [32]. Similarly, fabricated PVDF-NMP exhibited discontinuities as it has large macrovoids which plausibly gave rise to a relatively low dielectric strength. Although finger-like cavities were observed in the morphology of PVDF-DMF (Fig. 4f), its dielectric strength was found to be the highest. This could possibly be due to the fact that the bulk of its structure consisting of a uniform sponge-like sublayer. Since morphology is the key factor in determining the dielectric strength of a membrane [32], it would be expected that PVDF-TEP would have the highest dielectric strength. However, the dielectric strength of PVDF-TEP is lower than that of PVDF-DMF. It was suggested previously that membranes that had high electric breakdown field were also able to withstand greater elongation before mechanical failure [32]. PVDF-TEP displayed a lower tensile strain at break as compared to PVDF-DMF as shown in Table 2, which is consistent with the lower dielectric strength of PVDF-TEP. It is known that dielectric strength and mechanical properties of materials follow the weakest-link theory [39, 40]. From the results, the membranes that endured greater extension before mechanical fracture were also able to withstand greater force by electric fields. Fig. 6 shows a linear relationship between the dielectric strength and the tensile strain at break which is in agreement with the previous study [32]. Since the intrinsic properties of polymers are the key factors in affecting their mechanical properties [41], comparison between mechanical and electric breakdown behaviours could only be made for membranes with same material [32]. Thus, commercial UF-Synder was not included in Fig. 6 as it was made up of two different materials.

From the analysis above, it can be concluded that short finger-like cavities with sponge-like sublayer resulted in high dielectric strength and outstanding mechanical properties. This was followed by sponge-like structure with moderate dielectric strength, whilst large macrovoids or non-woven substrate layers led to low dielectric strength. Moreover, the results suggest that dielectric strength of the membranes could be inferred from their tensile tests as there was a linear correlation between dielectric strength and tensile strain at break.

3.2. Piezoelectric properties and crystalline structure of PVDF membranes

Piezoelectric properties of the membranes at nanoscales were characterized by PFM. Both out-of-plane (OP) and in-plane (IP) piezo-response could be imaged by PFM. Since the anti-fouling behaviour of piezoelectric membrane is dependent on the OP piezoelectric response [9], only OP PFM was performed. Topography, PFM amplitude and PFM phase images of unpoled UF-Synder, PVDF-DMF, PVDF-NMP and PVDF-TEP can be found in Fig. S3 under Supporting Information. The PFM amplitude and PFM phase profiles along the red line marked on the PFM images in Fig. S3 are displayed in Fig. S4 under Supporting Information. The PFM amplitude profiles illustrate that the amplitude ranges of PVDF-DMF, PVDF-NMP and PVDF-TEP were similar while the amplitude range of UF-Synder was wider. The PFM phase profiles show that the phase varied between −90° and 90° horizontally across the scan area for all the membranes. This indicates that the domains in these membranes were randomly orientated.

Piezoelectric response spectroscopy was performed with 10 × 10 points on the scan area of 2 μm × 2 μm. Since the range of DC bias sweep performed was limited by the capability of the instrument, not all the points generated a hysteresis loop (e.g. Fig. 1). These points corresponded to areas of weak piezoelectric response and larger DC bias sweep might be required to produce the hysteresis loops. The number of points where hysteresis loops were observed is listed in Table 2. The piezoelectric coefficient d_{33} was calculated for points that generated hysteresis loop using Eq. (1). Average d_{33} value and surface roughness for each membrane sample are also indicated in Table 2. Among the membranes, commercial UF-

Synder had the greatest error bar which implies that there was a wide variance in d_{33} values within the membrane.

Fig. shows a comparison of the FTIR spectra of the unpoled commercial and fabricated PVDF membranes from 1500 to 400 cm^{-1}. The presence of absorption peaks, at 1275, 840, 510 and 447 cm^{-1}, indicate the presence of β and γ phases in UF-Synder while no distinct peak, representing α phase, could be observed [42]. Prominent absorption peaks at 1209, 1148, 975, 763 and 613 cm^{-1} denote the existence of α phase in PVDF-TEP with weaker peaks of β and γ phases [42]. PVDF-DMF and PVDF-NMP show similar trend in their FTIR spectra where absorption peaks of α, β and γ phases could be seen. The different crystalline phases among the membranes were also supported by the X-ray diffraction (XRD) spectra, which could be found in Fig. S1.

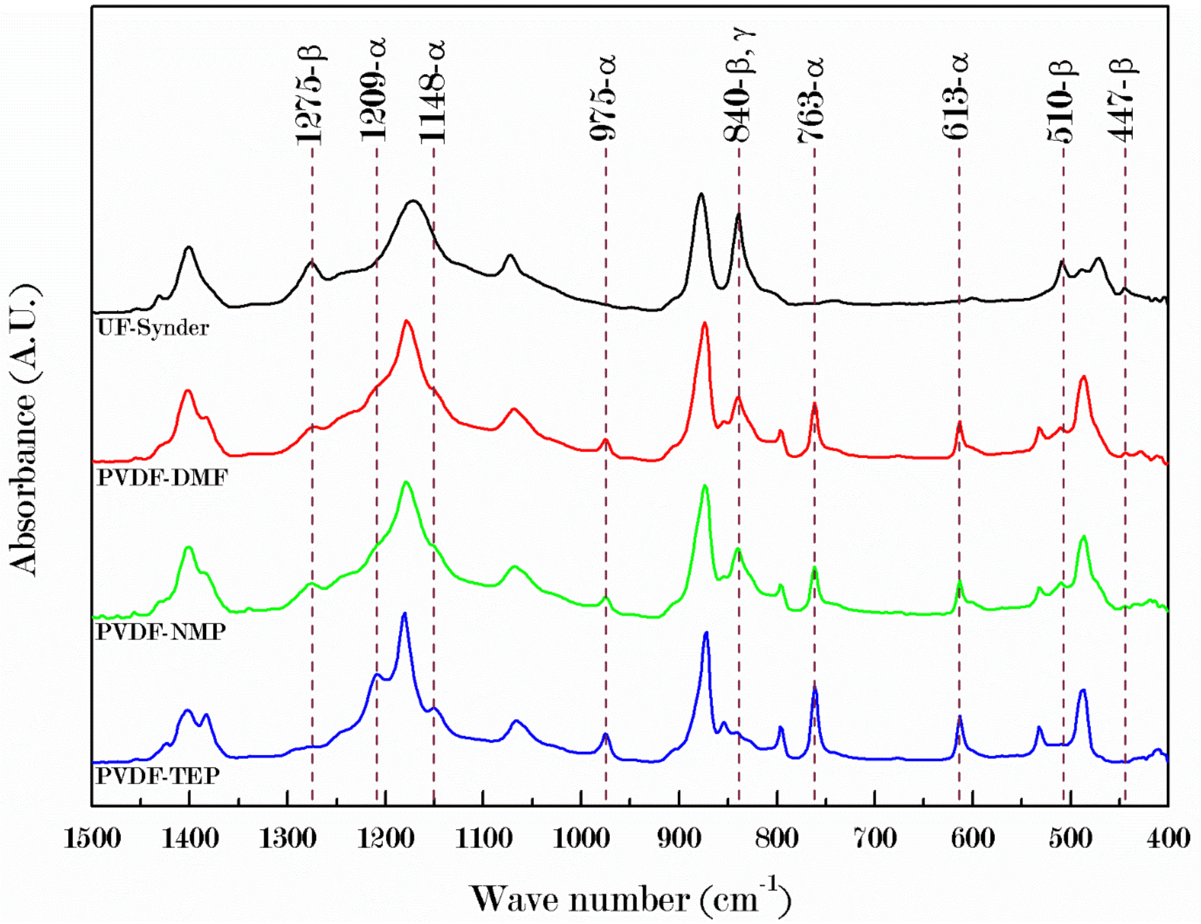

Fig. 7: FTIR spectra of unpoled commercial and fabricated PVDF membranes.

To quantify the proportion of β phase in each membrane, $F(\beta)$ was calculated using Eq. (2) as mentioned in section 2.3.4. The average $F(\beta)$ for each membrane is specified in Table 2. The results for $F(\beta)$ are in agreement with the FTIR spectra shown in Fig.. UF-Synder, with prominent β phase peaks, has the greatest $F(\beta)$ while PVDF-TEP has the lowest $F(\beta)$. A FESEM image of top surface of UF-Synder (Fig. 4a) shows the presence of uniform spherulites which possibly contributed to UF-Synder having the highest $F(\beta)$. By comparing the results obtained for d_{33} values and $F(\beta)$ for the membranes, a correlation could be identified. Fig. 8 reveals that the higher the $F(\beta)$, the greater the d_{33} value. This finding is consistent with the notion that the β phase in PVDF contributes to its electroactive properties [12]. Intuitively, piezoelectric properties of PVDF membranes can be enhanced by increasing its $F(\beta)$. In ascending order of d_{33} and $F(\beta)$ values, the degree of piezoelectric attributes for the membranes examined were PVDF-TEP, PVDF-DMF, PVDF-NMP and UF-Synder.

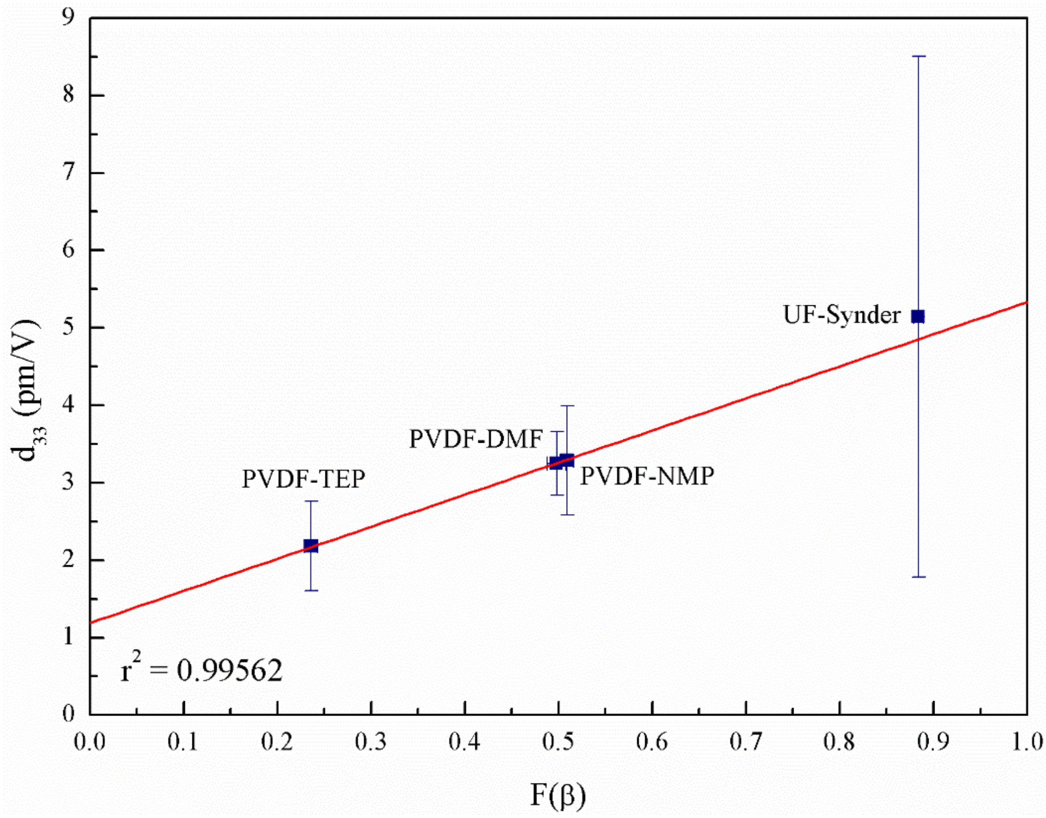

Fig. 8: Plot of average piezoelectric coefficient d_{33} against fraction of β phase $F(\beta)$ for unpoled commercial and fabricated PVDF membranes.

Based on the results above, UF-Synder has the greatest number of points where hysteresis loops were observed, highest d_{33} and largest $F(\beta)$. However, UF-Synder has the lowest dielectric strength. Out of the three fabricated PVDF membranes, PVDF-DMF had the most number of points where hysteresis loops were observed. PVDF-DMF and PVDF-NMP displayed similar d_{33} and $F(\beta)$ values.

3.3. Effect of electrical poling on properties of PVDF membranes

The commercial and fabricated PVDF membranes were subjected to electrical poling experiments to explore the possibility of enhancing the piezoelectric properties of the membranes. However, as mentioned earlier in section 2.4, commercial UF-Synder and fabricated PVDF-NMP membranes do not withstand high electric fields. For these membranes, the electric field was lowered such that electrical breakdown did not occur. The poling conditions of the membranes are listed in Table 1. The poling voltage used was much lower than the electrical breakdown voltage at room temperature because the electrical breakdown voltage reduces as temperature increases [32]. Hence, the poling voltage was set such that electrical breakdown did not occur at the increased temperature used during poling.

Contrary to previous studies [6, 43], electrical poling did not significantly change the microstructure of PVDF-NMP membrane. This could be possibly due to the lower electric field applied to this membrane during poling. The presence of macrovoids in PVDF-NMP limited the electric field that could be applied. On the other hand, visible differences could be observed between unpoled and poled PVDF-DMF or PVDF-TEP membranes. Instead of the finger-like cavities in the unpoled PVDF-DMF as shown in Fig. 4f, the cavities were drop-like after poling (Fig. 4h). Although the cavities were shorter, the thickness of the PVDF-DMF was similar before and after poling. One possible explanation for the drastic change in morphology of the cross-section is the alignment of electric dipoles in the direction of electric field. Fig. 9 illustrates a schematic diagram for the proposed explanation of the change in morphology during poling.

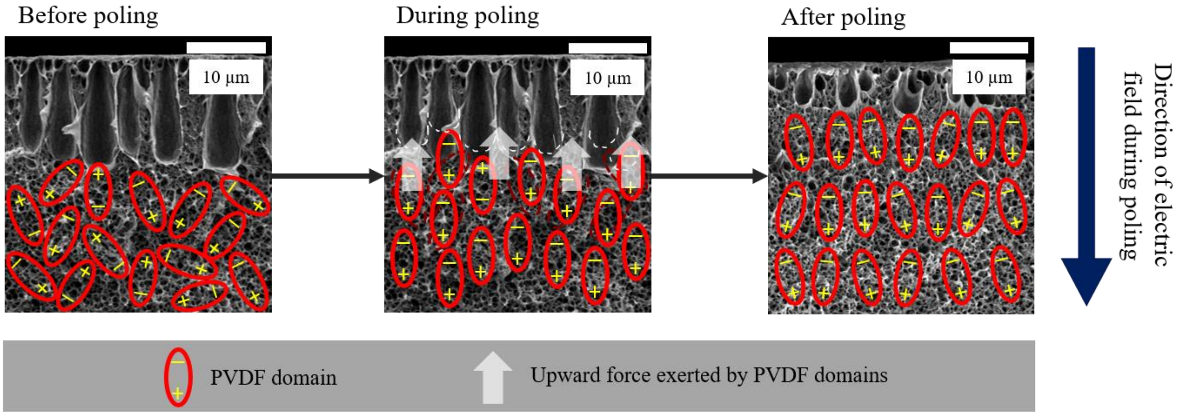

Fig. 9: Schematic diagram of the proposed explanation of the change in morphology in cross-section of PVDF-DMF before and after poling. The red oval-shaped symbol represents the PVDF dipole domains and the light gray arrow represents the force exerted by the PVDF dipole domains.

Prior to poling, the electric dipole domains were randomly orientated in the membrane structure. During poling, the electric dipoles gradually aligned themselves in the direction of the electric field. It is proposed that as the dipoles rotated, they exerted a force on the other dipoles above them. The dipoles, that were closer to the finger-like cavities, were more "free" than those in the sublayer. As the dipoles beneath them were aligned, these dipoles exerted a force on the boundaries of the cavities. Due to the alignment, the membrane was stretched and the cavities shrank in depth. It can be seen from Fig. 4h that the membrane near the cavities appeared to be stretched in the direction that is parallel to the direction of electric field. This is similar to the finding from previous study that there was possibly stretching force exerted on the membrane during poling [6]. The cavities did not disappear completely, probably because of the intensity of electric field was insufficient to achieve that. After poling, two distinct layers could be observed in cross-section FESEM image of poled PVDF-TEP in Fig. 4p. Even though unpoled PVDF-TEP exhibited asymmetrical structure that was denser nearer to the top surface, it was a gradual change in the void density across its cross-section. Similar to PVDF-DMF, the change in morphology of poled PVDF-TEP could be attributed to the alignment of nether electric dipoles during poling where they exerted a force on the upper dipoles which potentially compacted the top layer of the PVDF-TEP membranes. This resulted in two distinct layers of the poled PVDF-TEP. The electric field applied to PVDF-DMF and PVDF-TEP membranes during poling was identical at 10 MV/m.

Fig. 10 shows the topography, PFM amplitude and PFM phase images of unpoled and poled UF-Synder, PVDF-DMF, PVDF-NMP and PVDF-TEP. It is important to note that similar scan settings were used − for all the scans and that the scales of PFM images were consistent among the unpoled and poled membranes. The 3D topography images could be found in Fig. S2. The regions that are vibrant in PFM amplitude images signify greater tip deflection which in turn means higher amplitude of vibration, and vice versa. From the comparison between the topography and PFM amplitude images, bright PFM amplitude regions exist in both the dull and vibrant parts of the topography image. Hence, it could be substantiated that the topography had negligible effect on the PFM amplitude signals obtained. The PFM amplitude and phase images of the UF-Synder and PVDF-NMP membranes were similar before and after poling. This means that poling did not alter the piezoelectric behaviours of these membranes at nanoscales. This could be possibly due to the fact that electric field applied to these membranes during poling was insufficient. In contrast, the PFM amplitude images of poled PVDF-DMF and PVDF-TEP were more vibrant as compared to that of the unpoled which implies that poled PVDF-DMF and PVDF-TEP presented more areas with higher amplitudes of vibration in response to the applied biases. Fig. 10l also suggests that the dipole domains were mainly aligned in a single direction for poled PVDF-DMF as there is less contrast in its PFM phase image.

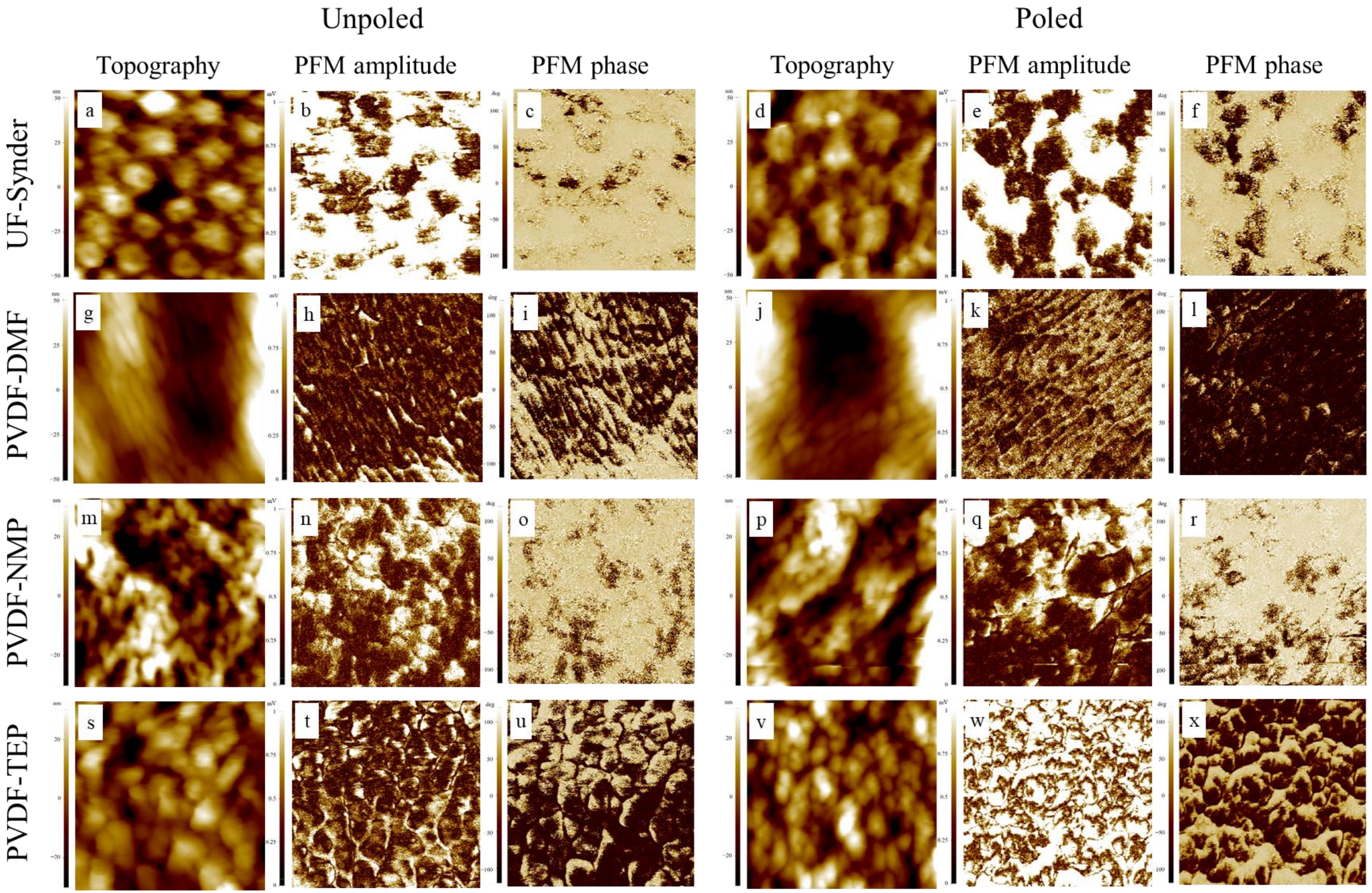

Fig. 10: Topography, PFM amplitude and PFM phase images of unpoled UF-Synder (a, b and c), poled UF-Synder (d, e and f), unpoled PVDF-DMF (g, h and i), poled PVDF-DMF (j, k and l), unpoled PVDF-NMP (m, n and o), poled PVDF-NMP (p, q and r), unpoled PVDF-TEP (s, t and u) and poled PVDF-TEP (v, w and x).

Besides the changes observed from FESEM and PFM images on poling, there were also changes in the other properties, which are summarized in Table 2. Similar trends were observed for the fabricated PVDF membranes before and after poling. Firstly, the pore diameter and porosity became smaller which would impact on their permeability (see also next section). This agrees with previous studies where it was found that electrical poling decreased pore size and hydraulic permeability of commercial PVDF membranes [8, 32]. Since EP characterization is based on Kelvin equation which is increasingly accurate for determining pore sizes ranging from 4 nm to 150 nm, EP may not be able to accurately detect pores larger than 150 nm. The significant porosity reduction for PVDF-NMP membranes was likely attributed by the smaller pores whilst the size of the larger pores remained relatively unchanged. Hence, there is negligible difference between the FESEM images of PVDF-NMP membrane before and after poling as shown in Fig. 4. Fig. S5 compares the mass-based pore size distribution of unpoled and poled PVDF-DMF membranes. It can be seen that the largest pore diameter reduced from 255 nm to 235 nm and the mass percentages of smaller pore sizes (5 nm to 100 nm) generally increased. This further confirms that electrical poling aligned the dipoles and reduced the size of large cavities or pores. Secondly, the thickness of the membrane was slightly reduced, possibly because of the compression force exerted by the weight of the top electrode whilst the membrane was at an elevated temperature. Thirdly, the piezoelectric properties and $F(\beta)$ were improved which is in agreement with Darestani et al. [6] who reported more prominent β phase absorption peaks and increased d_{33} value after poling. Lastly, consistent with a previous study [8], the surface became smoother. This was perhaps due to heat and compression during poling that smoothens the surface. A smoother surface is more favorable for membrane separation purposes as foulants tend to adhere to a greater extent to rough surface [44, 45]. Hence, electrical poling could have an additional function in smoothening the surface of membranes. Although commercial UF-Synder indicated outstanding d_{33} and $F(\beta)$ values, it had the lowest dielectric strength and this limited the electric field that could be applied during poling. Contrary to the fabricated membranes, the pore diameter and porosity of UF-Synder became larger after poling which enhanced its permeability. Moreover, the average d_{33} and $F(\beta)$ of UF-Synder remained fairly similar after poling. The mechanical properties of unpoled and poled membranes are listed in Table 2. Generally, the Young's modulus and tensile strength at break increased after poling except that for PVDF-TEP, and the tensile strain at break decreased slightly after poling. After poling, the morphology of the PVDF-TEP membranes consists of two distinct layers as shown in the FESEM images (Fig. 4). The worse mechanical properties of poled PVDF-TEP could possibly be explained by its layered morphology.

3.4. Filtration performance

The effect of applying an AC electrical signal (10 Vpp, 500 Hz) on the critical flux of silica particle for unpoled and poled PVDF membranes was explored. Flux stepping experiments were performed where the flux was increased at an interval of 20 L/m^2.h and each flux step lasted for 20 mins. The rate of TMP increase (dTMP/dt) at each flux was determined. According to the definition of critical flux, its flux value corresponds to the highest flux for dTMP/dt = 0; thus the x-intercept of the dTMP/dt vs. flux plot (Fig. 11) gives the value of critical flux. The critical flux of silica particles determined at different conditions are tabulated in Table 3. For all the fabricated membranes, the critical flux values increased for poled membranes with AC applied during filtration compared to controls, i.e., poled membrane without AC applied during filtration and unpoled membrane with/without AC applied during filtration. For example, the critical flux value for PVDF-DMF showed the greatest increase of 46%, while the increases were 34% and 25% for PVDF-NMP and PVDF-TEP, respectively. Meanwhile, for commercial UF-Synder, a slight difference in the critical values were observed for unpoled and poled membranes (<15%), but no change in the critical flux values regardless of AC application. First, the change in microstructure after poling was likely the reason to impact the critical flux value between unpoled and poled UF-Synder. This could be substantiated by the permeability of UF-Synder was greatly increased from an average of 1287 L/m^2.h.bar to 2117 L/m^2.h.bar (Table 2). Second, the application of AC signal showed negligible effect on critical flux value as the non-woven support of UF-Synder does not possess piezoelectric properties, which might result in the ineffective electrical poling or limited the overall micro-vibration effect of poled UF-Synder under AC signal.

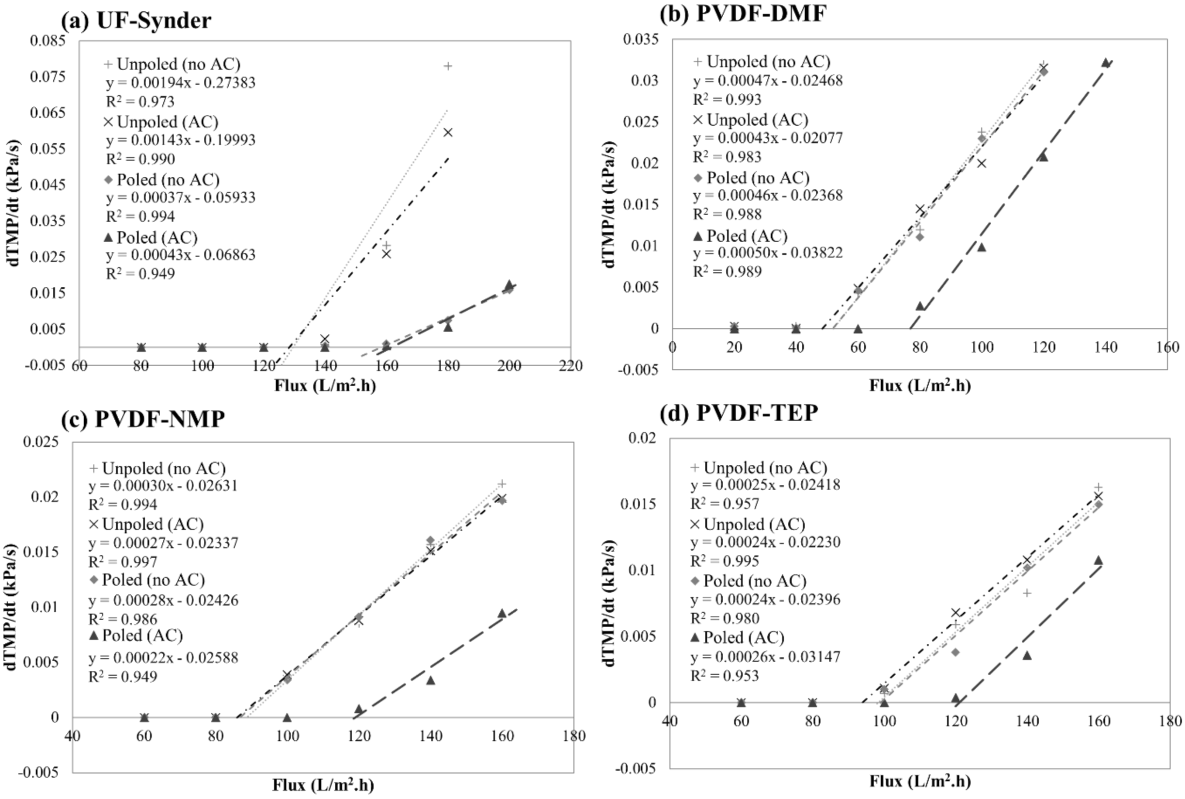

Fig. 11: Plot of dTMP/dt (kPa/s) vs. flux (L/m^2.h) for flux stepping experiments of unpoled and poled commercial and fabricated membranes (a) UF-Synder, (b) PVDF-DMF, (c) PVDF-NMP and (d) PVDF-TEP with and without AC signal (10 Vpp, 500 Hz) applied during filtration. Experimental conditions: 200 mg/L silica feed solution, cross-flow velocity of 0.1 m/s.

Table 3: Critical flux values for unpoled and poled commercial and fabricated membranes without and with an AC signal (10 Vpp, 500 Hz) applied during filtration.

Membrane	Application of AC	Critical flux (L/m^2.h)	Membrane	Application of AC	Critical flux (L/m^2.h)
Unpoled UF-Synder	No	141.1 ± 5.3	Unpoled PVDF-DMF	No	52.5 ± 2.7
Unpoled UF-Synder	Yes	139.8 ± 3.5	Unpoled PVDF-DMF	Yes	48.3 ± 3.3
Poled UF-Synder	No	160.4 ± 0.6	Poled PVDF-DMF	No	51.5 ± 3.4
Poled UF-Synder	Yes	159.6 ± 1.6 (+ 0%)[b]	Poled PVDF-DMF	Yes	76.4 ± 3.9 (+ 46%)[b]
Unpoled PVDF-NMP	No	87.7 ± 1.5	Unpoled PVDF-TEP	No	96.7 ± 3.5
Unpoled PVDF-NMP	Yes	86.6 ± 1.8	Unpoled PVDF-TEP	Yes	92.9 ± 2.8
Poled PVDF-NMP	No	86.6 ± 3.7	Poled PVDF-TEP	No	99.8 ± 3.8
Poled PVDF-NMP	Yes	117.6 ± 5.5 (+ 34%)[b]	Poled PVDF-TEP	Yes	121.0 ± 2.9 (+ 25%)[b]

[b] These values refer to the percentage increase in critical flux of poled membranes.

Based on the improvement in critical flux values, the PVDF-DMF was selected for longer fouling test to confirm the improvement in filtration performance. The operating flux was set at 150 L/m^2.h (~2 times higher than the critical flux value for poled membrane) and crossflow of 0.1 m/s and 200 mg/L silica solution was used as model foulant. The normalized TMP profiles are illustrated in Fig. 12.

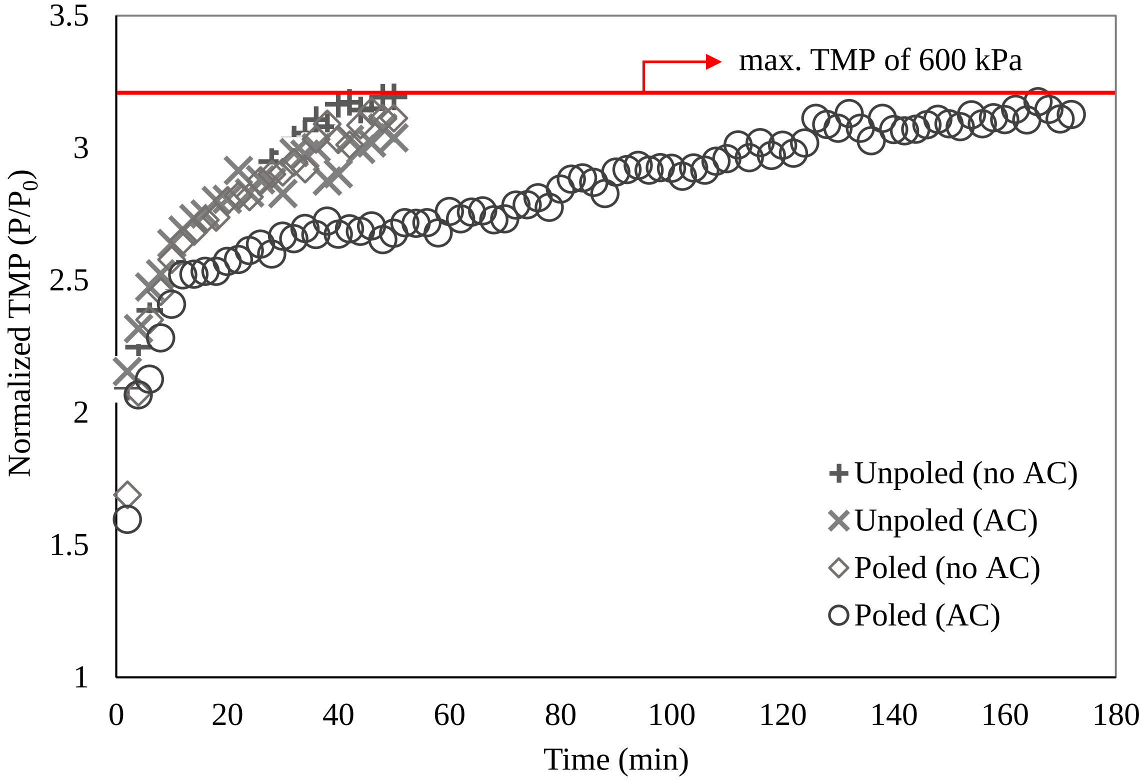

Fig. 12: Effect of AC signal (10 Vpp, 500 Hz) on normalized TMP (P/P_0) of unpoled and poled PVDF-DMF membranes during filtration of 200 mg/L silica solution at fixed permeate flux of 150 L/m^2.h and cross-flow velocity of 0.1 m/s.

Our results validated that the application of electrical signal improved the filtration performance of poled fabricated membranes but not that of unpoled membranes as shown in Fig. 12, similar to previous findings [5, 22]. The poled PVDF-DMF under AC signal (10 Vpp, 500 Hz) took ~175 mins (or dTMP/dt = 0.8 kPa/min) to reach the TMP of 600 kPa, i.e., maximum pressure attained by the pump, vs. ~55 mins for the controls, which corresponded to a remarkable improvement in the filtration duration by a factor of approximately three. The piezoelectric vibrations of poled PVDF-DMF disturbed the silica fouling layer with less prominent foulant layer enclosing areas of non-fouled spaces (Fig. 13d), while large chunks of foulant layers are observed for controls (Fig. 13a, b and c); thus resulted in lower cake resistance.

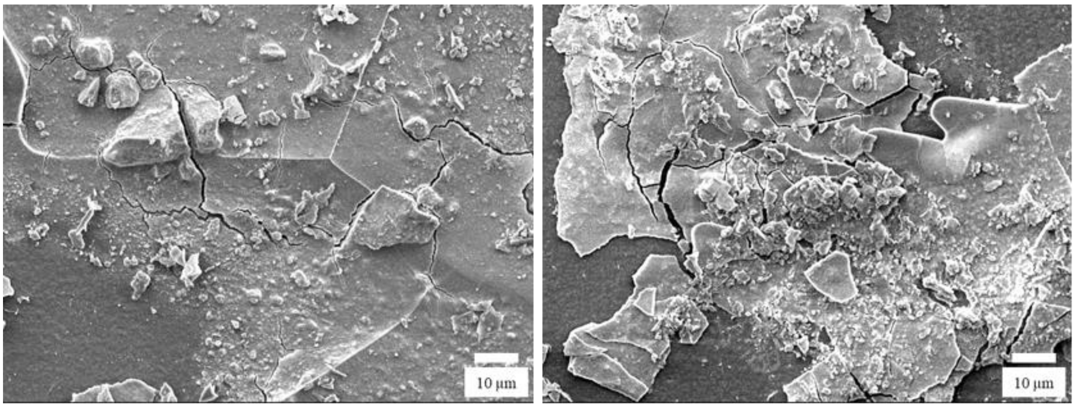

(a) Unpoled PVDF-DMF (no AC) (b) Unpoled PVDF-DMF (AC)

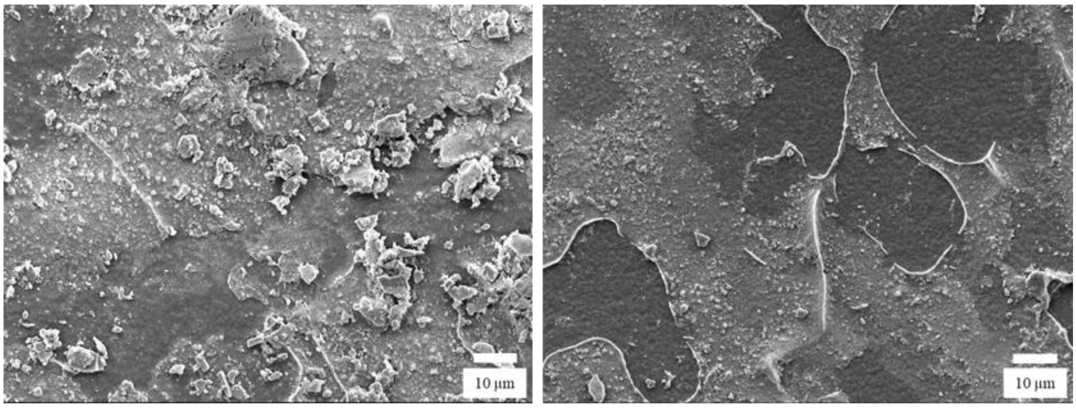

(c) Poled PVDF-DMF (no AC) (d) Poled PVDF-DMF (AC)

Fig. 13: FESEM images of fouled unpoled and poled PVDF-DMF membranes with or without application of AC signal (10 Vpp, 500 Hz) at 1 000 times magnification.

4. Conclusion

The effect of morphology on the performance of piezoelectric PVDF membranes was investigated. PVDF membranes were fabricated using DMF, NMP and TEP solvents. The different compatibility of these solvents for PVDF resulted in various membrane morphologies. Dielectric strength analysis and PFM showed that PVDF-DMF membranes, with finger-like cross-section morphology, had better dielectric and piezoelectric behaviour among all the fabricated membranes. Although commercial UF-Synder membranes displayed outstanding, intrinsic, piezoelectric properties, it had a low dielectric strength and its critical flux did not improve after poling at mild conditions. Thus, besides possessing superb piezoelectric properties, it was also crucial for an ideal piezoelectric PVDF membrane to have the appropriate morphology that was suitable for electrical poling. Morphologies, such as macrovoids and distinctive layers, resulted in low dielectric strength which was undesirable for electrical poling. The results from piezoelectric response spectroscopy indicated that electrical poling aligned the dipoles and enhanced the piezoelectric properties of the fabricated PVDF membranes. Electrical poling also reduced the size of the finger-like cavities in PVDF-DMF membrane as illustrated by FESEM while minimal change was observed for PVDF-NMP membrane. Flux stepping experiments showed piezoelectric vibrations of poled membranes under the application of electrical signals dramatically enhanced critical flux by 25 to 46%. Filtration fouling test on PVDF-DMF membranes further demonstrated poled PVDF-DMF under electrical signal delayed fouling progression (66% reduction in dTMP/dt), and thus extending filtration duration by a factor of approximately three.

Nomenclature

d_{33}	Piezoelectric coefficient
$F(\beta)$	Fraction of β phase
A_α	Absorbance value at 763 cm^{-1}
A_β	Absorbance value at 840 cm^{-1}
K_α	Absorption coefficient of α (6.1×10^4 $cm^2.mol^{-1}$)
K_β	Absorption coefficient of β (7.7×10^4 $cm^2.mol^{-1}$)
m_{wet}	Mass of the wetted membrane before pore draining
m_{dry}	Mass of the dry membrane
ρ_w	Density of the wetting liquid
ρ_m	Density of the membrane
h	Film thickness
U	Rolling speed
η	Dynamic viscosity of the solution at atmospheric pressure

Acknowledgements

The financial support of the Economic Development Board (EDB) of Singapore to the Singapore Membrane Technology Centre (SMTC), Nanyang Environment & Water Research Institute (NEWRI) is greatly appreciated. We thank Professor William B. Krantz for assistance with evapo-porometry characterization.

References

[1] F. Zamani, J. W. Chew, E. Akhondi, W. B. Krantz and A. G. Fane, "Unsteady-state shear strategies to enhance mass-transfer for the implementation of ultrapermeable membranes in reverse osmosis: A review," *Desalination,* vol. 356, pp. 328-348, 2015.

[2] A. I. Zouboulis and M. D. Petala, "Performance of VSEP vibratory membrane filtration system during the treatment of landfill leachates," *Desalination,* vol. 222, pp. 165-175, 3 2008.

[3] S. Ahmed, M. G. Rasul, M. A. Hasib and Y. Watanabe, "Performance of nanofiltration membrane in a vibrating module (VSEP-NF) for arsenic removal," *Desalination,* vol. 252, pp. 127-134, 3 2010.

[4] W. Shi and M. M. Benjamin, "Effect of shear rate on fouling in a Vibratory Shear Enhanced Processing (VSEP) RO system," *Journal of Membrane Science,* vol. 366, pp. 148-157, 1 2011.

[5] H. G. L. Coster, T. D. Farahani and T. C. Chilcott, "Production and characterization of piezo-electric membranes," *Desalination,* vol. 283, pp. 52-57, 2011.

[6] M. T. Darestani, H. G. L. Coster, T. C. Chilcott, S. Fleming, V. Nagarajan and H. An, "Piezoelectric membranes for separation processes: Fabrication and piezoelectric properties," *Journal of Membrane Science,* vol. 434, pp. 184-192, 2013a.

[7] M. T. Darestani, T. C. Chilcott and H. G. L. Coster, "Piezoelectric membranes for separation processes: Operating conditions and filtration performance," *Journal of Membrane Science,* vol. 435, pp. 226-232, 2013b.

[8] M. T. Darestani, T. C. Chilcott and H. G. L. Coster, "Separation performance of PVDF membranes poled in intense electric fields," *Separation and Purification Technology,* vol. 118, pp. 604-611, 2013c.

[9] H. Coster, M. Darestani and T. C. Chilcott, Membrane and separation system, 2010.

[10] H. Kawai, "The Piezoelectricity of Poly (vinylidene Fluoride)," *Japanese Journal of Applied Physics,* vol. 8, pp. 975-976, 7 1969.

[11] J. Mulder, Basic Principles of Membrane Technology, 2nd ed., Springer Netherlands, 1996.

[12] V. V. Kochervinskii, "Piezoelectricity in crystallizing ferroelectric polymers: Poly(vinylidene fluoride) and its copolymers (A review)," *Crystallography Reports,* vol. 48, pp. 649-675, 01 7 2003.

[13] Y. Zhang, L. Ye, W. Zhao, L. Chen, M. Zhang, G. Yang and H. Zhang, "Antifouling mechanism of the additive-free -PVDF membrane in water purification process:

Relating the surface electron donor monopolarity to membrane-foulant interactions," *Journal of Membrane Science,* vol. 601, p. 117873, 3 2020.

[14] A. Salimi and A. A. Yousefi, "Analysis Method: FTIR studies of β-phase crystal formation in stretched PVDF films," *Polymer Testing,* vol. 22, pp. 699-704, 2003.

[15] M. Nasir, H. Matsumoto, T. Danno, M. Minagawa, T. Irisawa, M. Shioya and A. Tanioka, "Control of diameter, morphology, and structure of PVDF nanofiber fabricated by electrospray deposition," *Journal of Polymer Science Part B: Polymer Physics,* vol. 44, pp. 779-786, 2006.

[16] M. N. a. F. B. a. L. I. a. A. B. a. C. Lacabanne, "Structural evolution of PVDF during storage or annealing," *Polymer,* vol. 45, pp. 1679 - 1688, 2004.

[17] H. Shaik, S. N. Rachith, K. J. Rudresh, A. S. Sheik, K. H. Thulasi Raman, P. Kondaiah and G. Mohan Rao, "Towards β-phase formation probability in spin coated PVDF thin films," *Journal of Polymer Research,* vol. 24, p. 35, 09 2 2017.

[18] T. Hattori, M. Kanaoka and H. Ohigashi, "Improved piezoelectricity in thick lamellar β-form crystals of poly(vinylidene fluoride) crystallized under high pressure," *Journal of Applied Physics,* vol. 79, pp. 2016-2022, 1996.

[19] Y. Ye, Y. Jiang, Z. Wu and H. Zeng, "PHASE TRANSITIONS OF POLY(VINYLIDENE FLUORIDE) UNDER ELECTRIC FIELDS," *Integrated Ferroelectrics,* vol. 80, pp. 245-251, 2006.

[20] R. G. Jr and N. C. P. Souza Nociti, "Effect of PMMA addition on the solution crystallization of the alpha and beta phases of poly(vinylidene fluoride) (PVDF)," *Journal of Physics D: Applied Physics,* vol. 28, p. 432, 1995.

[21] M. S. a. S.-S. N., "Investigation of the crystalline structure of PVDF in PVDF/PMMA/graphene polymer blend nanocomposites," *Polymer Composites,* vol. 32, pp. 1451 - 1460, 2011.

[22] D. Chen and C. Pomalaza-Ráez, "A self-cleaning piezoelectric PVDF membrane system for filtration of kaolin suspension," *Separation and Purification Technology,* vol. 215, pp. 612-618, 2019.

[23] J. Bae, I. Baek and H. Choi, "Efficacy of piezoelectric electrospun nanofiber membrane for water treatment," *Chemical Engineering Journal,* vol. 307, pp. 670-678, 2017.

[24] S. Gee, B. Johnson and A. L. Smith, "Optimizing electrospinning parameters for piezoelectric PVDF nanofiber membranes," *Journal of Membrane Science,* vol. 563, pp. 804-812, 2018.

[25] J. K. Krinks, M. Qiu, I. A. Mergos, L. K. Weavers, P. J. Mouser and H. Verweij, "Piezoceramic membrane with built-in ultrasonic defouling," *Journal of Membrane Science,* vol. 494, pp. 130-135, 11 2015.

[26] H. Mao, M. Qiu, J. Bu, X. Chen, H. Verweij and Y. Fan, "Self-Cleaning Piezoelectric Membrane for Oil-in-Water Separation," *ACS Applied Materials & Interfaces,* vol. 10, 5 2018.

[27] H. Mao, J. Bu, M. Qiu, D. Ding, X. Chen, H. Verweij and Y. Fan, "PZT/Ti composite piezoceramic membranes for liquid filtration: Fabrication and self-cleaning properties," *Journal of Membrane Science,* vol. 581, pp. 28-37, 2019.

[28] P. Cao, J. Shi, J. Zhang, X. Wang, J. T. Jung, Z. Wang, Z. Cui and Y. M. Lee, "Piezoelectric PVDF membranes for use in anaerobic membrane bioreactor (AnMBR) and their antifouling performance," *Journal of Membrane Science,* vol. 603, p. 118037, 5 2020.

[29] M. L. Yeow, Y. T. Liu and K. Li, "Morphological study of poly(vinylidene fluoride) asymmetric membranes: Effects of the solvent, additive, and dope temperature," *Journal of Applied Polymer Science,* vol. 92, pp. 1782-1789, 2004.

[30] G. R. Guillen, Y. Pan, M. Li and E. M. V. Hoek, "Preparation and Characterization of Membranes Formed by Nonsolvent Induced Phase Separation: A Review," *Industrial & Engineering Chemistry Research,* vol. 50, pp. 3798-3817, 2011.

[31] M.-m. Tao, F. Liu, B.-r. Ma and L.-x. Xue, "Effect of solvent power on PVDF membrane polymorphism during phase inversion," *Desalination,* vol. 316, pp. 137-145, 2013.

[32] M. T. Darestani, T. C. Chilcott and H. G. L. Coster, "Changing the microstructure of membranes using intense electric fields: Dielectric strength studies," *Journal of Membrane Science,* vol. 452, pp. 367-378, 2 2014.

[33] J. Rinaldo Gregorio and M. Cestari, "Effect of crystallization temperature on the crystalline phase content and morphology of poly(vinylidene fluoride)," *Journal of Polymer Science Part B: Polymer Physics,* vol. 32, pp. 859-870, 4 1994.

[34] W. B. Krantz, A. R. Greenberg, E. Kujundzic, A. Yeo and S. S. Hosseini, "Evapoporometry: A novel technique for determining the pore-size distribution of membranes," *Journal of Membrane Science,* vol. 438, pp. 153-166, 2013.

[35] R. Wang, L. Shi, C. Y. Tang, S. Chou, C. Qiu and A. G. Fane, "Characterization of novel forward osmosis hollow fiber membranes," *Journal of Membrane Science,* vol. 355, pp. 158-167, 2010.

[36] A. Bottino, G. Camera-Roda, G. Capannelli and S. Munari, "The formation of microporous polyvinylidene difluoride membranes by phase separation," *Journal of Membrane Science,* vol. 57, pp. 1-20, 4 1991.

[37] J. C. a. J. Z. a. L. Z. a. G. S. O. a. T.-S. Chung, "Using green solvent, triethyl phosphate (TEP), to fabricate highly porous PVDF hollow fiber membranes for membrane distillation," *Journal of Membrane Science,* vol. 539, pp. 295 - 304, 2017.

[38] M. Smeeth, H. A. Spikes and S. Gunsel, "The Formation of Viscous Surface Films by Polymer Solutions: Boundary or Elastohydrodynamic Lubrication?," *Tribology Transactions,* vol. 39, pp. 720-725, 1 1996.

[39] J. Blok and D. G. LeGrand, "Dielectric Breakdown of Polymer Films," *Journal of Applied Physics,* vol. 40, pp. 288-293, 1 1969.

[40] C. Zweben and B. W. Rosen, "A statistical theory of material strength with application to composite materials," *Journal of the Mechanics and Physics of Solids,* vol. 18, pp. 189-206, 6 1970.

[41] S. Y. Hong and M. Kertesz, "Theoretical evaluation of Young's moduli of polymers," *Phys. Rev. B,* vol. 41, no. 16, pp. 11368-11378, 6 1990.

[42] X. Cai, T. Lei, D. Sun and L. Lin, "A critical analysis of the α, β and γ phases in poly(vinylidene fluoride) using FTIR," *RSC Advances,* vol. 7, pp. 15382-15389, 2017.

[43] M. T. Darestani, T. C. Chilcott and H. G. L. Coster, "Effect of poling time on filtration properties of PVDF membranes treated in intense electric fields," *Polymer Bulletin,* vol. 71, pp. 951-964, 01 4 2014a.

[44] E. M. V. Hoek, S. Bhattacharjee and M. Elimelech, "Effect of Membrane Surface Roughness on Colloid---Membrane DLVO Interactions," *Langmuir,* vol. 19, pp. 4836-4847, 2003.

[45] L. Chen, Y. Tian, C.-q. Cao, J. Zhang and Z.-n. Li, "Interaction energy evaluation of soluble microbial products (SMP) on different membrane surfaces: Role of the reconstructed membrane topology," *Water Research,* vol. 46, pp. 2693-2704, 2012.